[J] CBM_Eng Characteristics_Q1_2019

by Sri Atmaja Rosyidi

Submission date: 04-Jun-2019 12:33AM (UTC+0700)
Submission ID: 1139558858
File name: J_CBM_Eng_Characteristics_Q1_2019.pdf (6.22M)
Word count: 10658
Character count: 50442

Construction and Building Materials 204 (2019) 781–799

Contents lists available at ScienceDirect

Construction and Building Materials

journal homepage: www.elsevier.com/locate/conbuildmat

Engineering characteristics of nanosilica/polymer-modified bitumen and predicting their rheological properties using multilayer perceptron neural network model

Nur Izzi Md. Yusoff [a,*], Dhawo Ibrahim Alhamali [a], Ahmad Nazrul Hakimi Ibrahim [a], Sri Atmaja P. Rosyidi [b], Norhidayah Abdul Hassan [c]

[a] Smart and Sustainable Township Research Centre, Universiti Kebangsaan Malaysia, Bangi, Malaysia
[b] Dept. of Civil Engineering, Universitas Muhammadiyah Yogyakarta, Yogyakarta, Indonesia
[c] Faculty of Civil Engineering, Universiti Teknologi Malaysia, Skudai, Malaysia

HIGHLIGHTS

- We study the effect of nano-silica modified bitumen in unaged and aged conditions.
- NS-PMB6 improves the viscoelastic properties and resistance to the ageing.
- The ANN models show a good agreement between measured and predicted data.

ARTICLE INFO

Article history:
Received 5 October 2018
Received in revised form 7 January 2019
Accepted 27 January 2019

Keywords:
Polymer-modified bitumen (PMB)
Nanosilica
Chemical
Microstructure
Rheology
Artificial neural network (ANN)

ABSTRACT

This study examines the effect of mixing varying percentages of nano-silica (NS), i.e. 2, 4 and 6% (by weight of polymer-modified bitumen, PMB) with PMB, in unaged and aged conditions. The Fourier transform infrared spectroscopy, x-ray diffraction, scanning electron microscopy and dynamic shear rheometer were used to determine chemical, microstructure and rheological properties of the binders, respectively. An artificial neural network (ANN) model, known as the multilayer perceptron neural networks model with three different algorithms namely; Levenberg-Marquardt (LM), scaled conjugate gradient (SCG), and gradient descent with adaptive back propagation (GDA) were used to predict the rheological properties of binders. The results indicate that adding NS to PMB may weaken the binders and delay their ageing. The amorphous structures of NS-PMBs remain unchanged and no new crystalline phase was formed when varying percentages of NS was added to PMB. Extreme heat caused a marked increase in the complex modulus of NS-PMB6 while low temperatures reduced its complex modulus. This resulted in enhanced resistance to the rutting and fatigue parameters. Adding higher amounts of NS particles to PMB also improved the viscoelastic properties and resistance to the ageing conditions of NS-PMB6. In terms of modeling, it was found that the most suitable algorithms and neurons number in the hidden layer for the ANN-Unaged model is LM algorithm and 11 neurons. For ANN-RTFOT and ANN-PAV models, the optimum algorithms and neurons number in hidden layer is SGC algorithm with 11 neurons and LM with 9 neurons respectively. The R-value (>0.95) for all models show a good agreement between measured and predicted data. It was concluded that the ANNs could be used as an accurate, fast and practical method for researchers and engineers to predict the phase angle and complex modulus of NS-PMBs.

1. Introduction

The past several years have seen an increase in the demand for high-quality bitumen to meet the need for durable pavements with low maintenance and rehabilitation expenses. In the search for superior quality bitumen, more and more investigations have been focusing on bitumen modification. Amongst the methods investigated for modifying bitumen, the most frequently used method is polymer modification. The modification of bitumen with polymer, widely known as polymer-modified bitumen (PMB), requires that the polymer be incorporated into the bitumen via mechanical mixing or chemical reaction [1]). For the past four decades, researchers have been giving more focus on PMB, and, since the 1970 s, many research articles have been published on this area of research [2].

* Corresponding author.
E-mail addresses: izzi@ukm.edu.my (N.I Md. Yusoff), hnorhidayah@utm.my (N. Abdul Hassan).

https://doi.org/10.1016/j.conbuildmat.2019.01.203
0950-0618/

Among the polymers used in these studies are plastomers (e.g. polyethylene (PE), polypropylene (PP), ethylene–vinyl acetate (EV ethylene–butyl acrylate (EBA)) and thermoplastic elastomers (e.g. styrene–butadiene–styrene (SBS), styrene–isoprene–styrene (SIS), and styrene– ethylene/butylene–styrene (SEBS)), all of which were originally intended for modifying bitumen [3–7]. These polymers have been shown to produce a certain degree of provement in the characteristics of bitumen, such as enhanced stiffness at high temperature, better cracking resistance at low temperature, superior moisture resistance, and longer fatigue life [8–11].

Despite of these successes, researchers still have to find methods to reduce production cost; reduce the sensitivity of some of the PMB to high temperatures; improve ageing resistance and poor storage stability; as well as enhance the binders' elasticity [12]. Nanotechnology is being used more frequently to modify bitumen in the attempt to eliminate the drawbacks of PMBs. ce then, several researchers have proven that nano-materials such as nano-clay, nano-hydrated lime, and nano-carbonate very effective in enhancing the engineering properties of bituminous binders and asphalt mixtures [13–15]). The advantage of using this nano-material is its high performance and low cost of production [16]. Nano-silica composites have been rec ng a lot of attention in the field of science. Nano-silica has a large surface area, good adsorption, good dispersal ability, high chemical purity, and excellent stability [17]. The advantages of these nano-materials are by virtue of in their low manufacturing cost and superior performance [16,18]

On the other hand, the need to model and estimate the damage accumulated over the service life of a new binder based on the empirical rutting and cracking performance model is another issue that must be addressed. Since an artificial neural network (ANN) is successful used in several civil engineering problems such as tide forecasting, earthquake-induced liquefaction, and wave-induced seabed instability that are difficult to solve or interrupt through conventional approaches of engineering mechanics. ANN models can provide reasonable accuracy in dealing with civil engineering problems and is a more effective tool for engineering applications. Several types of research have been conducted in the last decade to develop a prediction model by using the ANN method [19,20]. Ceylan et al. [19] described the development of a new asphalt mixture dynamic modulus |E*| prediction model which use the ANN method. In addition, Kok l. [20] conducted a study with the objective of modeling the complex modulus of base and Styrene-butadiene-styrene (SBS) modified bitumens by using ANNs.

Thus, this current study was divided into two se ns. The first section is to examine the effect of mixing varying percentages of nano-silica (NS), i.e. 2, 4 and 6% (by weight of polymer-modified bitumen, PMB) with PMB, in unaged and aged conditions. The physical testings (i.e. penetration, ductility, softening point) rage stability test, Fourier transform infrared spectroscopy (FTIR), X-Ray diffraction (XRD), scanning electron microscopy (SEM) and dynamic shear rheometer (DSR) were used to determine the physical, chemical, microstructure and rheological properties of the binders, respectively. In additi for the second section, a new and efficient approach to predict the rheological properties of NS-PMBs such as complex modulus and phase angle via the multilayer perceptron neural networks model is presented. In this s dy, the NS content, temperature and frequency for determining the complex modulus and phase angle were evaluated using both experimental and modeling approach.

2. Experimental design

2.1. Materials and sample preparation

The material employed in the present research is PG-76 polymer-modified bitumen, which also serves as the control sample. Table 1 shows the physical and rheological characteristics of the control sample. The tropical regions of the world have a consistent climate and are able to provide the supply of performance grade (PG) binder. Nano-silica (NS) particles in the form of white powder with a maximum size of approximately 32 nm were used in varying percentages to modify PMB in the laboratory. The PMB was modified with 2, 4 and 6% NS by weight of binder

The NS and bitumen were blended at a shear rate of 3000 revolutions per minute (rpm) for one hour at a constant high temperature of 163 °C. The bitumen sample was prepared in laboratory by modifying the NS. Three different NS concentrations, namely 2, 4 and 6% (by weight of PMB), were added to the PMB binders. The NS materials were mixed in a high shear rate machine. Floating bubbles could be observed on the surface of bituminous binder once the NS has dispersed and liquefied in the PMB binder. The physical and storage stability properties of the control and NS-PMBs have shown in Table 2.

2.2. X-Ray diffraction

The X-RD is a very fundamental experimental technique and is frequently used to identify the crystal structure of solids; this include lattice constant and geometry, determination of unknown materials, orientation of a crystal, preferred orientation of polycrystals, defects, stress, etc. In this research, the X-Ray Diffraction (X-RD) was performed using a Brucker axs-D8 diffractometer to determine the crystal and microstructure of the NS particles and NS-PMB's binders by using Cu k radiation ($\lambda = 0.15406$ nm; 40 kV, 40 mA). The scanned range is between 5° and 80° in the 2θ with a scanning rate of 0.025 o/s.

2.3. Fourier transform Infrared spectroscopy

Infrared absorption spectroscopy is one of the most effective methods for detecting and identifying organic compounds. It is

Table 1
Physical and rheological properties of PG-76.

Test Quality Specification	Test Standard	Unit	Requirement	Result
Softening Point	ASTM D36 [21]	°C	Min. 70 °C	93
Penetration	ASTM D5 [22]	0.1 mm	Min. 45	46
Flash Point	AASHTO T48	°C	Min. 260 °C	343
Performance Specification				
Viscosity at 135 °C	ASTM D4402 [23]	Pa.s	Max. 3 Pa.s	2.45
Dynamic shear, G*/sin δ Test temp. @ 10 rad/s, 76 °C	AASHTO T315	kPa	Min. 1.00 kPa	2.10
Rolling Thin Film Oven Test Residue (AASHTO T240)				
Mass Loss	AASHTO T240	%	Max. 1.00%	0.04
Dynamic shear, G*/sin δ Test temp. @ 10 rad/s, 76 °C	AASHTO T315	kPa	Min. 2.20 kPa	3.40
Pressure Ageing Vessel Residue (AASHTO R28)				
PAV Ageing Test Temperature			100 °C	
Dynamic shear, G*/sin δ Test temp. @ 10 rad/s, 76 °C	AASHTO T315	kPa	Min. 5000 kPa	1200

Table 2
Physical properties of PMB and NS-PMBs.

Test/Sample	Penetration @ 25 °C (d-mm)	Penetration Index (PI)	Ductility @ 25 °C (cm)	Softening Point (°C)	Storage Stability
Test Standard	ASTM D5 [22]	–	ASTM D113 [24]	ASTM D36[21]	–
PMB	66.40	4.11	102.00	73.00	–
NS-PMB2	59.40	4.09	81.00	75.00	Stable
NS-PMB4	49.50	3.55	93.00	76.00	Stable
NS-PMB6	38.20	4.02	108.00	83.00	Unstable

able to identify the vibrational structure of the molecules as well as the molecular structure of the various functional groups. The Fourier Transform Infrared Spectroscopy (FTIR) was used to analyse the functional characteristic of the bituminous binders and was performed using the PerkinElmer Spectrum 400 FTIR / FTNIR. Samples were analysed using the Attenuated Total Reflectance (ATR) between the range of 4000 and 650 cm^{-1}.

2.4. Morphology analysis

The morphology of NS-PMBs binders was investigated using the Hitachi VP-SEM SU 3500. Scanning electron microscope (SEM) is frequently used to examine the physical and chemical characteristics of nano-materials. The electron beam was scanned directly on the surface of the samples and this produces various signals which were then analysed. Three different operations can be used with the SEM, namely secondary electron imaging (SEI), backscattered electron imaging (BSE), and energy dispersive x-ray (EDX). In this research, the BSE and EDX were employed to determine surface morphology as well as to analyse the characteristics of the microstructure of the PMB and NS-PMBs binders. BSE is able to produce visual information which distinguishes the different intensity of the chemical phase. High-energy electrons are utilized directly on the specimen to backscatter the electrons. The number of electrons reflected is the atomic number of the sample. SEM can also be used to identify the elements making up a sample by using the X-ray spectrum of a specific specimen. This analysis can be done in a spot mode which allows for the navigation and focus on a specific area of the specimen.

2.5. Ageing procedure

PMB and NS-PMBs were aged under artificial conditions using a rolling thin film oven test (RTFOT) where short term ageing was carried out at 163 °C for 85 min. Long term ageing was done in a pressure ageing vessel (PAV) where the binders were placed in the oven under 2.1 MPa at 100 °C for 20 h. The RTFOT and PAV procedures were carried out as per ASTM D2872 [25] and ASTM D6521 [26], respectively.

2.6. Dynamic shear rheometer

The dynamic shear rheometer (DSR) was used to determine the rheological characteristics of the PMB and NS-PMB binders. The samples were immersed in water to control its temperature in the DSR. The fluid bath ensures that the sample temperature is uniform and constant throughout the test. The temperature control unit is used to maintain the temperature to within ±0.1 °C of the temperature suggested by SHRP. The strain sweep test for the unaged samples was performed at 46 °C to ensure that the rheological tests are conducted within the linear viscoelastic (LVE) region. The limit for LVE behaviour is the point beyond which the measured value of complex modulus is 95% of its zero-strain value. The frequency sweeps in DSR tests were done at varying temperatures. Therefore, the complex modulus and phase angle were measured at different temperatures and frequencies for different plate diameters and gap widths, as shown in Table 3.

Table 3
DSR test conditions for sample geometry.

Parameter	Testing Configuration 1	Testing Configuration 2
Temperature	15–45 °C	35–85 °C
Frequency	0.6283–62.83 rad/s	0.6283–62.83 rad/s
Plate diameter	8 mm	25 mm
Gap width	2 mm	1 mm

2.7. Artificial neural network modeling

This research used the MATLAB mathematical software version 7.11.0 (R2010b) as a tool for developing the ANN models and to predict the complex modulus and phase angle. The results of the experiment were used to develop the ANN prediction models. The method relies on the training part of the sample via the feed forward back propagation learning. The aim of this research is to find the best model which can be used to produce a satisfactory prediction for complex modulus and phase angle. The datasets from experimental results were used as the desired outputs (targets). Concentration, temperature and frequency were used as input parameters whilst complex modulus and phase angle were used as output parameter. The three-layer back propagation neural network models were developed using 1260 DSR data planned using the central composite design as training data. The dataset was divided into five subsets of training and testing sets, each time omitting one set for testing and another four sets for training. The dataset is used for training and is tested for the remaining sub-set in each training process, called the "fold cross validation".

The most popular training algorithm is the supervised back-propagation [27,28]. This research used the back-propagation algorithm to train the networks. The type of multilayer perceptron (MLP) artificial neural network used in this study consists of three layers, namely the input layer, the hidden layer, and the output layer. Each of these layers has several neurons. The number of neurons in the input and output layers are equal to the number of input and output variables. The activity of the neurons in the hidden layer is determined by the activities of the input units and the weight on the connections between the input and the hidden units. The performance of the output is determined by the activity of the hidden layer and the weights between the hidden and output layers [29]. The log-sigmoid transfer function (log-sig) was used between the hidden layers and the output layer in all developed ANN models. The non-linear nature of this function enhances the performance of the neural network.

The training algorithms, including the Levenberg Marquardt (LM), scaled conjugate gradient (SCG), and gradient descent with adaptive back propagation (GDA), were investigated and used in

Table 4
Neural network topologies of samples employed for the optimisation process.

Algorithm	Train-LM	Train-SCG	Train-GDA
Input layer	3	3	3
	5	5	5
Hidden layer	7	7	7
	9	9	9
	11	11	11
Output layer	2	2	2

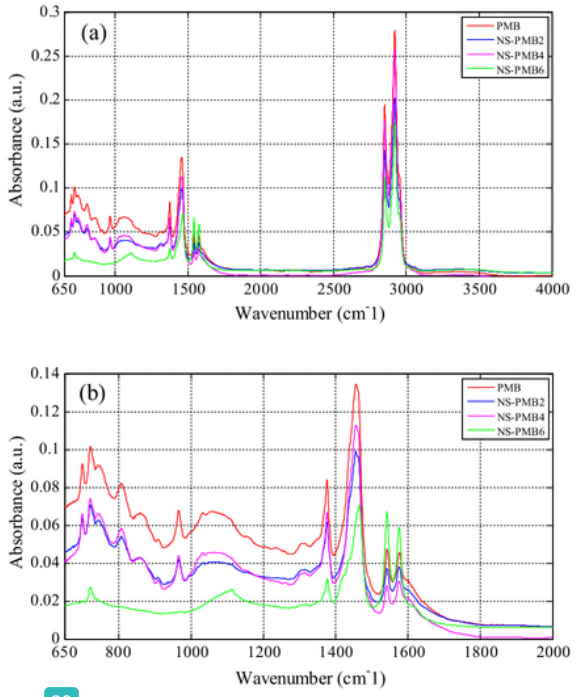

Fig. 1. Fourier Transform Infrared Spectroscopy (FTIR) for PMB and NS-PMBs binders.

Table 5
Assignations of the Main Bands of the FTIR Spectra.

Wavenumber (cm^{-1})	Assignations
2919	ν C—H of —(CH_3)—
2850	ν C—H of —(CH_2)—
1576	ν C=O conjugated
1542	ν C=C
1456	δ C—H of —$(CH_2)_n$—
1376	δ C—H of CH_3
1059	ν S=O sulfoxide
965	δ C—H trans di-substituted —CH=CH—
807	δ C—H aromatic mono-substituted
721	δ C—H aromatic mono-substituted
699	δ C—H aromatic mono-substituted

this study before optimising the ANN topology. A Log sigmoid transfer function was used for both the hidden and output layers of the ANN. During training, varying number of neurons (5, 7, 9, and 11) were applied for the hidden layer of the three training algorithms (LM, SCG, and GDA) tested, while the number of neurons in the input layer was kept constant at three as illustrated in Table 4. The optimal number of neurons in the hidden layer was selected based on the minimum mean square error (MSE) and maximum efficiency during the testing stage [30].

The performances of the five cross validation prediction models (5-FCV) were measured using a statistical criterion and a graphical representation based on the results of the network versus experimental data. The statistical criteria for the evaluation of the 5-FCV models in both the training and testing stages are Mean squared error (MSE) (Eq. (1)), Coefficient of efficient (COE) (Eq. (2)) and regression (Eqs. (3)–(5)).

$$MSE = \frac{1}{n}\sum_{i=1}^{n}(a,b)^2 \tag{1}$$

$$COE = 1 - \frac{\sum_{i=1}^{n}(a-b)}{\sum_{i=1}^{i+n}(a-b)} \tag{2}$$

$$Y = a + bX \tag{3}$$

$$b = \frac{N\sum XY - (\sum X)(\sum Y)}{N\sum X^2 - (\sum X)^2} \tag{4}$$

$$a = \frac{\sum Y - b\sum X}{N} \tag{5}$$

where N is the number of observation; X is the index, and Y is the size of data.

3. Results and discussion

3.1. FTIr

FTIR spectroscopy is a simple analytical technique and is commonly employed to investigate the chemical and structural changes that occur in different samples in order to determine the ageing of the modified bitumen [31]. In this research, FTIR was used to evaluate the microstructure of the modified bituminous binders. Fig. 1 shows the FTIR spectra of the PMB and NS-PMBs binders. Fig. 1(a) shows the identical assignations of the majority of the bands, with the strong peaks at around 2850 cm^{-1} and 2919 cm^{-1}, which is a common C–H stretching vibration in aliphatic chains [32].

Fig. 1(b) shows a clear disparity in characteristic bands, i.e. a partially enlarged spectra between 650 cm^{-1} and 2000 cm^{-1}. The band at 699 cm^{-1} is related to the bending of C—H aromatic mono-substituted of the styrene blocks and the band at 965 cm^{-1} is related to the bending of C—H trans di-substituted —CH=CH— of the butadiene block. The band at around 1059 cm^{-1} is related to the stretching of S=O sulfoxide. The aliphatic branched band (bending C—H of CH_3) and aliphatic index band (bending C—H of —$(CH_2)_n$—) are present at 1376 cm^{-1} and 1456 cm^{-1}, respectively. The 1542 cm^{-1} and 1576 cm^{-1} bands correspond with the aromatic band (stretching C=C aromatic) and carbonyl band (stretching C=O conjugated), respectively [17,32–34]). Table 5 shows the identical assignations.

Fig. 1(a) and (b) show the clear difference in the FTIR trends for PMB and NS-PMB binders between 699 cm^{-1} and 1576 cm^{-1}. This indicates the altered microstructure of NS-PMBs binders in comparison to the PMB binder. The peak area ratios of the bands were used to estimate the change in chemical bonding, and computation was done using Eqs. (6)–(11) [17,32–34]. The changes in the bands ratio are presented in Table 6.

Table 6
Change in the Ratio of the Bands in NS-PMB's binders.

Sample	CH=CH 965 cm^{-1}	S=O 1059 cm^{-1}	C—H of CH_3 1376 cm^{-1}	C—H of —$(CH_2)_n$— 1456 cm^{-1}	C=C 1542 cm^{-1}	C=O 1576 cm^{-1}
PMB	0.066728	0.063519	0.034230	0.052049	0.015761	0.033418
NS-PMB2	0.040086	0.031235	0.044933	0.075471	0.022450	0.024160
NS-PMB4	0.030119	0.038328	0.041066	0.055659	0.017358	0.033820
NS-PMB6	0.053072	0.083131	0.048318	0.060314	0.050648	0.082426

$$I_{CH=CH} = \frac{\text{Area of the ethylene band centered around 966 cm}^{-1}}{\sum \text{Area of the spectral bands between 200 cm}^{-1} \text{ and 650 cm}^{-1}} \quad (6)$$

$$I_{S=O} = \frac{\text{Area of the sulfoxide band centered around 1059 cm}^{-1}}{\sum \text{Area of the spectral bands between 200 cm}^{-1} \text{ and 650 cm}^{-1}} \quad (7)$$

$$I_{HofCH3} = \frac{\text{Area of the aliphatic branched band centered around 1376 cm}^{-1}}{\sum \text{Area of the spectral bands between 200 cm}^{-1} \text{ and 650 cm}^{-1}} \quad (8)$$

$$I_{C-Hof-(CH2)n-} = \frac{\text{Area of the aliphatic index band centered around 1456 cm}^{-1}}{\sum \text{Area of the spectral bands between 200 cm}^{-1} \text{ and 650 cm}^{-1}} \quad (9)$$

$$I_{C=C} = \frac{\text{Area of the aromatic band centered around 1542 cm}^{-1}}{\sum \text{Area of the spectral bands between 200 cm}^{-1} \text{ and 650 cm}^{-1}} \quad (10)$$

$$I_{C=O} = \frac{\text{Area of the carbony band centered around 1576 cm}^{-1}}{\sum \text{Area of the spectral bands between 200 cm}^{-1} \text{ and 650 cm}^{-1}} \quad (11)$$

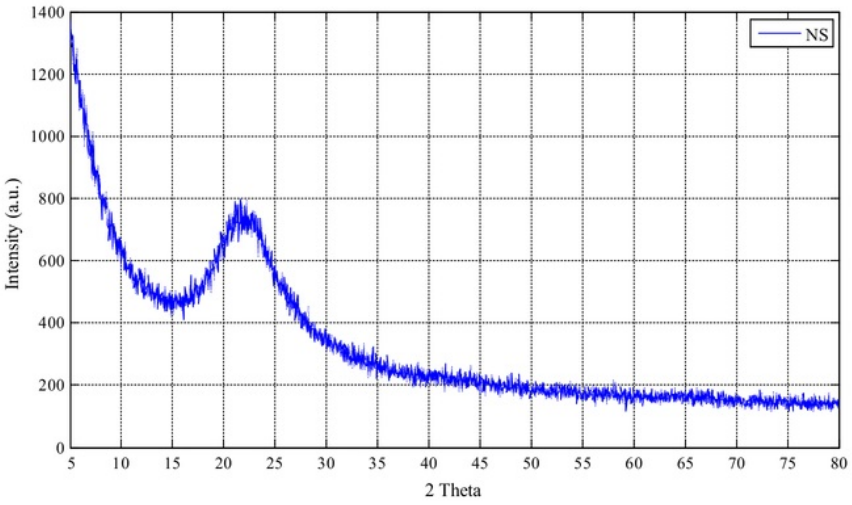

Fig. 2. X-RD patterns for NS particles.

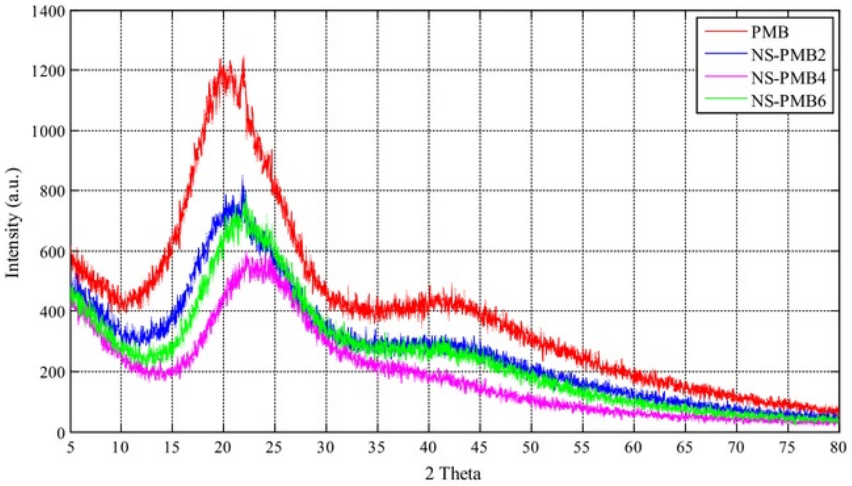

Fig. 3. X-RD patterns for PMB and NS-PMBs binders.

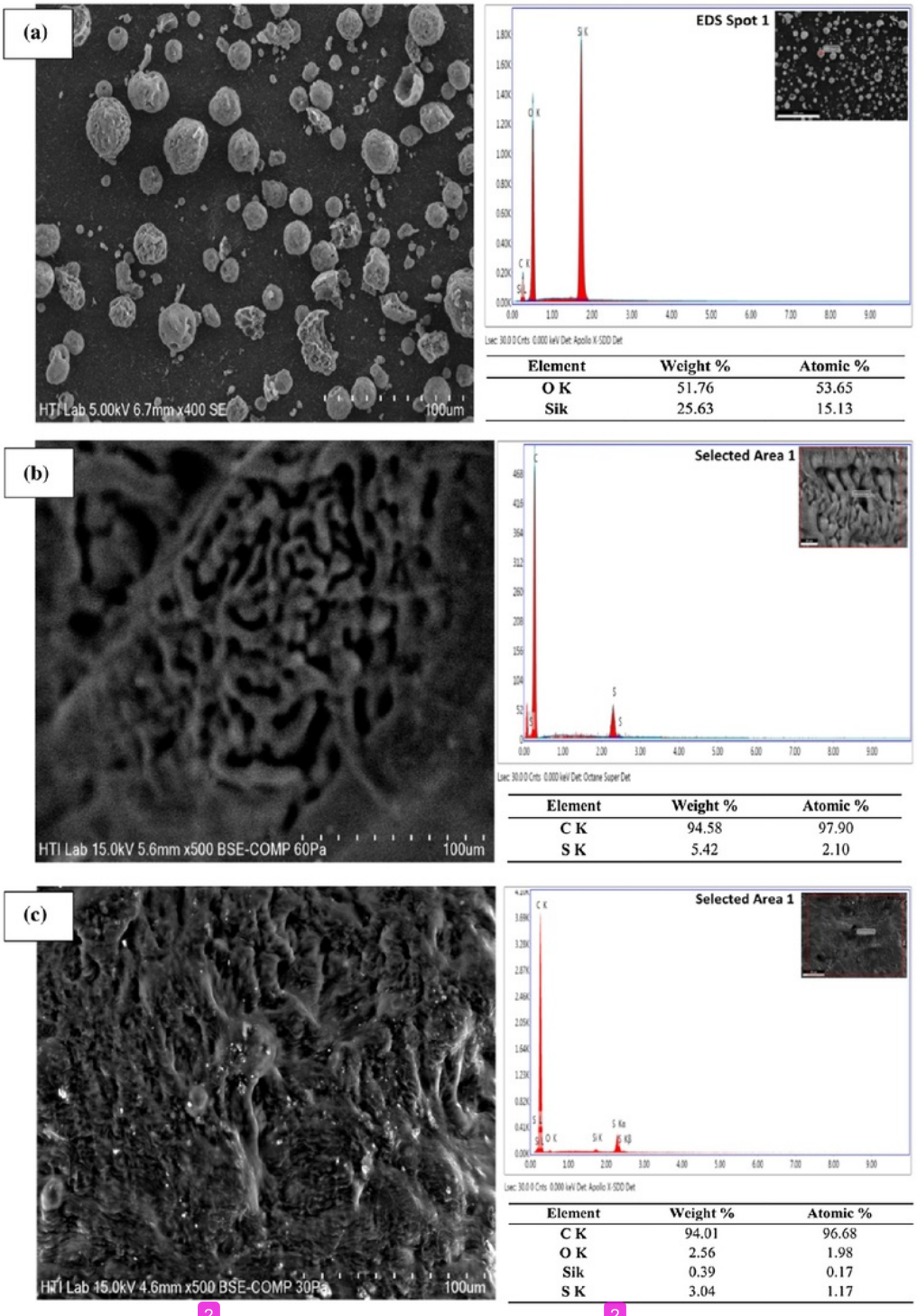

Fig. 4. SEM images of NS, PMB and NS-PMB. (a) SEM image of NS at 400× magnification with EDX analysis; (b) SEM image of PMB at 500× magnification with EDX analysis; (c) SEM image of NS-PMB2 at 500× magnification with EDX analysis; (d) SEM image of NS-PMB4 at 500× magnification with EDX analysis; and (e) SEM image of NS-PMB6 at 500× magnification with EDX analysis.

Table 6 shows the change in the ratio of the bands in the NS-PMBs binders, where the band for carbonyl (C=O) of the NS-PMB4 and NS-PMB6 increased after the addition of NS while the band for NS-PMB2 decreased. In addition, the aromatic indices (C=C) for NS-PMB2, NS-PMB4 and NS-PMB6 increased in comparison to that of the PMB. While the sulfoxide index (S=O) for NS-

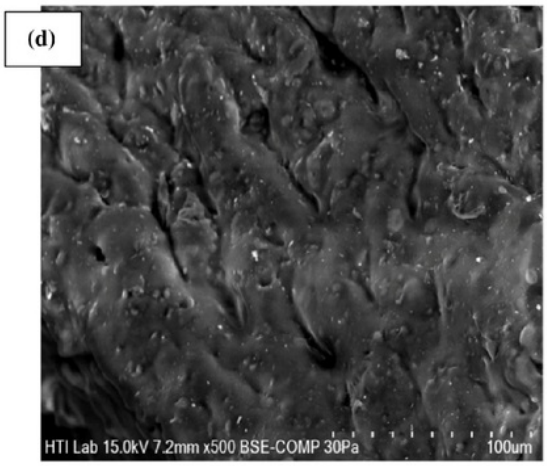

Element	Weight %	Atomic %
C K	90.02	93.89
O K	5.52	4.32
Sik	0.8	0.36
S K	3.66	1.43

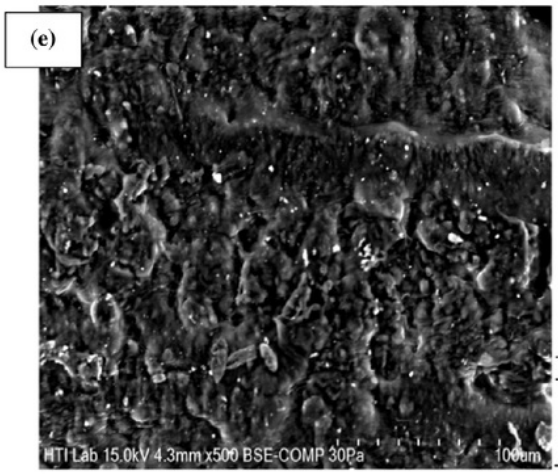

Element	Weight %	Atomic %
C K	91.39	95.08
O K	3.83	2.99
Sik	1.09	0.49
S K	3.68	1.44

Fig. 4 (*continued*)

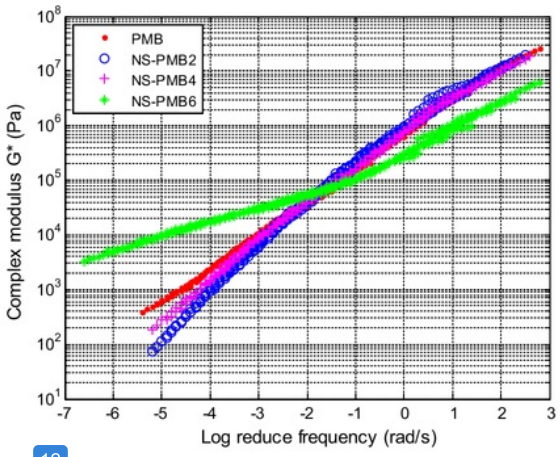

Fig. 5. Master curves of complex modulus at a reference temperature of 25 °C for PMB and NS-PMBs binders.

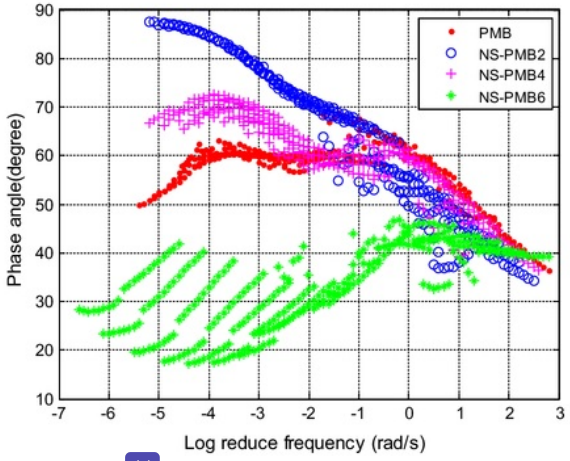

Fig. 6. Phase angle master curves at a reference temperature of 25 °C for PMB and NS-PMBs binders.

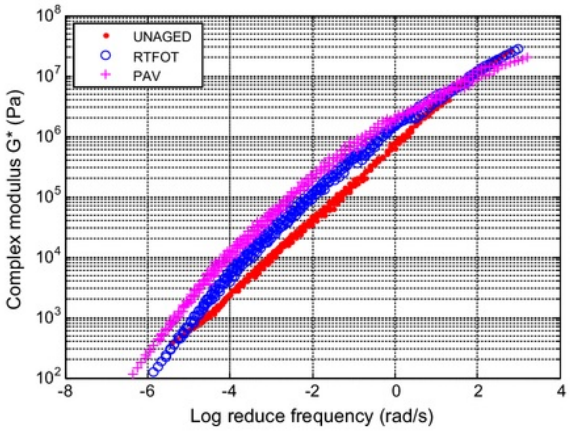

Fig. 7. Complex shear modulus master curves for PMB after RTFOT and PAV.

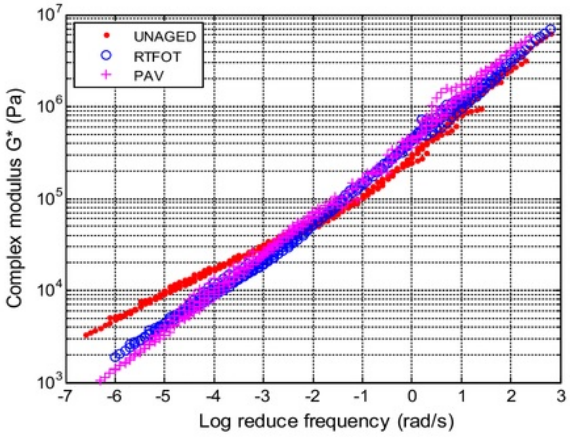

Fig. 8. Complex shear modulus master curves for NS-PMB6 after RTFOT and PAV.

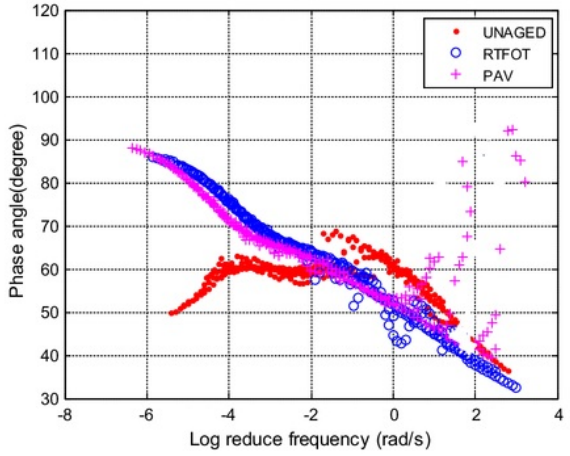

Fig. 9. Phase angle master curves for PMB after RTFOT and PAV.

PMB6 increased, the value for NS-PMB2 and NS-PMB4 decreased in comparison to PMB. Hence, the sulfoxide index is not a good indicator of ageing index; instead, the carbonyl index was chosen as

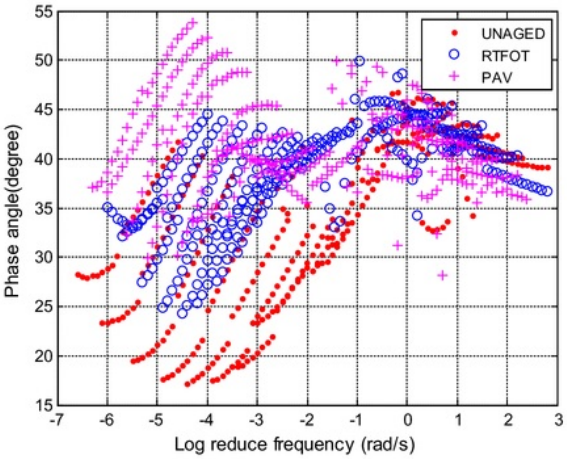

Fig. 10. Phase angle master curves for NS-PMB6 after RTFOT and PAV.

the ageing index [17]. Table 6 shows a general increase in the carbonyl index of NS-PMBs. This indicates that adding NS to PMB may weaken and delay the ageing process of bituminous binders.

3.2. X-Rd

The X-RD pattern shows that the PMB has an amorphous structure whereas NS particles are non-crystalline. The results of X-RD show that there is a reduction in intensity when 2, 4 and 6% NS were added to PMB. This indicates that the NS particles are well dispersed and uniformly distributed in the mixture. Figs. 2 and 3 show the typical peaks for the NS particles and the binders, respectively. Fig. 3 shows that the amorphous structures of NS-PMBs binders remain unchanged and no new crystalline phase was formed when varying amounts of NS were added to the PMB. Moreover, the addition of 3, 5 and 7% alumina nanoparticles (Al_2O_3) as a modifier for base bitumen produced similar results as when adding NS, in that no new peak was observed (non-crystalline) [35].

3.3. Morphology analysis

Scanning Electron Microscopy (SEM) and Energy Dispersive X-ray (EDX) analysis were done to determine the morphology of NS-PMBs, where the fineness and distribution of NS particles in PMB were examined. The images from SEM show that the microstructure of NS-PMBs binders was altered and that the NS particles were uniformly and regularly-dispersed in the phase of the PMB. Adding 2 and 4% NS caused the NS particles to agglomerate, and the addition of 6% NS resulted in a clear agglomeration in the NS-PMB6 binder. The findings of this research is similar with those made by Yao et al. [17] with regard to the evaluation of the morphology of nano-silica modified bitumen using SEM images. Analysis of the EDX results show that the NS-PMBs are made up of carbon (C k), sulphur (S k), silica (Si k) and oxygen (O k). Carbon and sulphur are associated mainly with PMB, whereas oxygen is related to NS. Moreover, the physical dispersion of NS in PMB, as shown in Fig. 4, indicates the increase in the amount of NS for NS-PMB2, NS-PMB4 and NS-PMB6.

3.4. Rheological properties of unaged binders

The master curve of complex modulus and phase angle in the present research was produced using T_{ref} = 25 °C, and a numerical method was employed to compute the shifting factors. Fig. 5 shows

the complex modulus for PMB and NS-PMBs master curves. A comparison of NS-PMB2 and NS-PMB4 show that the complex modulus is lower at high temperature and/or low frequency, while the complex modulus of NS-PMB6 shows a significant increase at high temperature and/or low frequency.

NS-PMB exhibits lower complex modulus at high frequency and/or low temperature. The addition of higher amount of NS particles to PMB improved the viscoelastic properties of NS-PMBs, as manifested by higher complex modulus at high temperatures and/or low frequency and low complex modulus at low temperature and/or high frequency. This is due to the hardness of NS particles which was identified through the penetration and softening point tests. Yao et al. [17] investigated the rheological properties of PG 58–34 bituminous binder modified with acrylonitrile-butadienestyrene (ABS) through the addition of NS particles. They found that the addition of NS particles decreased the complex modulus, a finding which is congruent with the results of this research.

Fig. 6 shows the phase angle master curves for the PMB and NS-PMBs binders, which are similar with the curve for NS-PMBs, with the exception of NS-MB6. The master curves for NS-PMB2 and NS-PMB4 show a higher increase in phase angle compared to the increase for PMB; this shows that a small amount of NS in the PMB matrix has a negative impact on the properties of bituminous binders, while higher amounts of NS improve the viscoelastic properties of NS-PMB, especially for those of NS-PMB6. In general, the curve is relatively smooth in comparison to the curve for NS-PMB6, with the phase angle master curve showing varying decrease in the phase angle with considerable discontinuity and presence of waves. The discontinuous waves in the master curves are an indication of the different chemical structures produced by the addition of varying percentages of NS. The only similarity in all phase angle master curves of the NS-PMBs is at the end of the high frequency. In general, NS-PMB6 shows the highest efficiency in terms of complex modulus and phase angle at all temperatures and frequencies. The NS-PMB6 also shows high complex modulus and low phase angle values, indicating a good rutting (permanent deformation) at high temperatures.

3.5. Rheological properties of aged binders

The master curves for the complex modulus of PMB and NS-PMB6 binders after RTFOT and PAV aging are shown in Figs. 7 and 8. The curves show that there is a difference in two regions in terms of the effect of ageing on NS-modified PMB; the first region is where the NS particles is dominant at low loading frequency and/or high temperature, while the second region is where the bituminous phase is dominant at high loading frequency and/or low temperature. In the region dominated by bitumen, the changes in the complex modulus of NS-PMB6 that are attributable to ageing are comparable that those observed in the unaged samples, with a slight increase in complex modulus after ageing. A slight decrease in complex modulus was observed in the region dominated by NS particles, which indicate that NS weakened the effect of ageing on PMB. It should be noted that NS could have reacted chemically with the PMB binder during mixing and heat-

Table 7
Statistical measure from the5-KCV training stage for fold 3 with various learning algorithms simulation between measured and examined unaged data.

K-FCV Learning Algorithms	Unaged Data: 5-FCV Training Stage with Fold (F = 3)					
	Output 1: Phase angle			**Output 2:** Complex modulus		
	MSE	R	COE	MSE	R	COE
LM [3–11–2]*	**0.017666**	**0.99442**	**0.98888**	**0.0080262**	**0.99728**	**0.99444**
LM [3–9–2]	0.019313	0.99333	0.98671	0.005672	0.99862	0.99722
LM [3–7–2]	0.022000	0.99134	0.98275	0.0077681	0.99743	0.99479
LM [3–5–2]	0.022403	0.99102	0.98211	0.013012	0.99288	0.98539
SCG [3–11–2]	0.02753	0.98641	0.97299	0.021475	0.97991	0.96021
SCG [3–9–2]	**0.029432**	**0.98444**	**0.96913**	**0.024534**	**0.97369**	**0.94807**
SCG [3–7–2]	0.025554	0.9883	0.97673	0.025551	0.9715	0.94368
SCG [3–5–2]	0.030324	0.98348	0.96723	0.026112	0.97022	0.94118
GDA [3–11–2]	**0.031229**	**0.98251**	**0.96524**	**0.02834**	**0.96505**	**0.93071**
GDA [3–9–2]	0.039058	0.97248	0.94563	0.029112	0.96343	0.92688
GDA [3–7–2]	0.052475	0.94977	0.90186	0.03183	0.95583	0.91259
GDA [3–5–2]	0.038275	0.97359	0.94779	0.029683	0.96135	0.92399

The bold values are shows the best model for different learning algorithms during training and testing stage.

Table 8
Statistical measures from the 5-KCV testing stage for fold 3 with different learning algorithms simulation between measured and examined unaged data.

K-FCV Learning Algorithms	Unaged Data : 5-FCV Testing Stage with Fold (F = 3)					
	Output 1: Phase angle			**Output 2:** Complex modulus		
	MSE	R	COE	MSE	R	COE
LM [3–11–2]*	**0.038406**	**0.97887**	**0.95576**	**0.015655**	**0.99004**	**0.97952**
LM [3–9–2]	0.069023	0.92686	0.85712	0.04686	0.90861	0.81653
LM [3–7–2]	0.061357	0.94907	0.8871	0.035063	0.95149	0.89728
LM [3–5–2]	0.051026	0.96206	0.92192	0.05817	0.85585	0.71728
SCG [3–11–2]	0.053409	0.95835	0.91445	0.05806	0.85366	0.71835
SCG [3–9–2]	**0.047061**	**0.96953**	**0.93358**	**0.030823**	**0.96133**	**0.92062**
SCG [3–7–2]	0.057144	0.95493	0.90207	0.034796	0.95122	0.89884
SCG [3–5–2]	0.074601	0.92304	0.83309	0.049522	0.8962	0.79509
GDA [3–11–2]	**0.058828**	**0.95423**	**0.89621**	**0.033397**	**0.95528**	**0.90681**
GDA [3–9–2]	0.073261	0.92439	0.83904	0.042301	0.92621	0.8505
GDA [3–7–2]	0.080994	0.9057	0.80326	0.031799	0.95716	0.91551
GDA [3–5–2]	0.065403	0.94524	0.87172	0.053559	0.87643	0.76033

The bold values are shows the best model for different learning algorithms during training and testing stage.

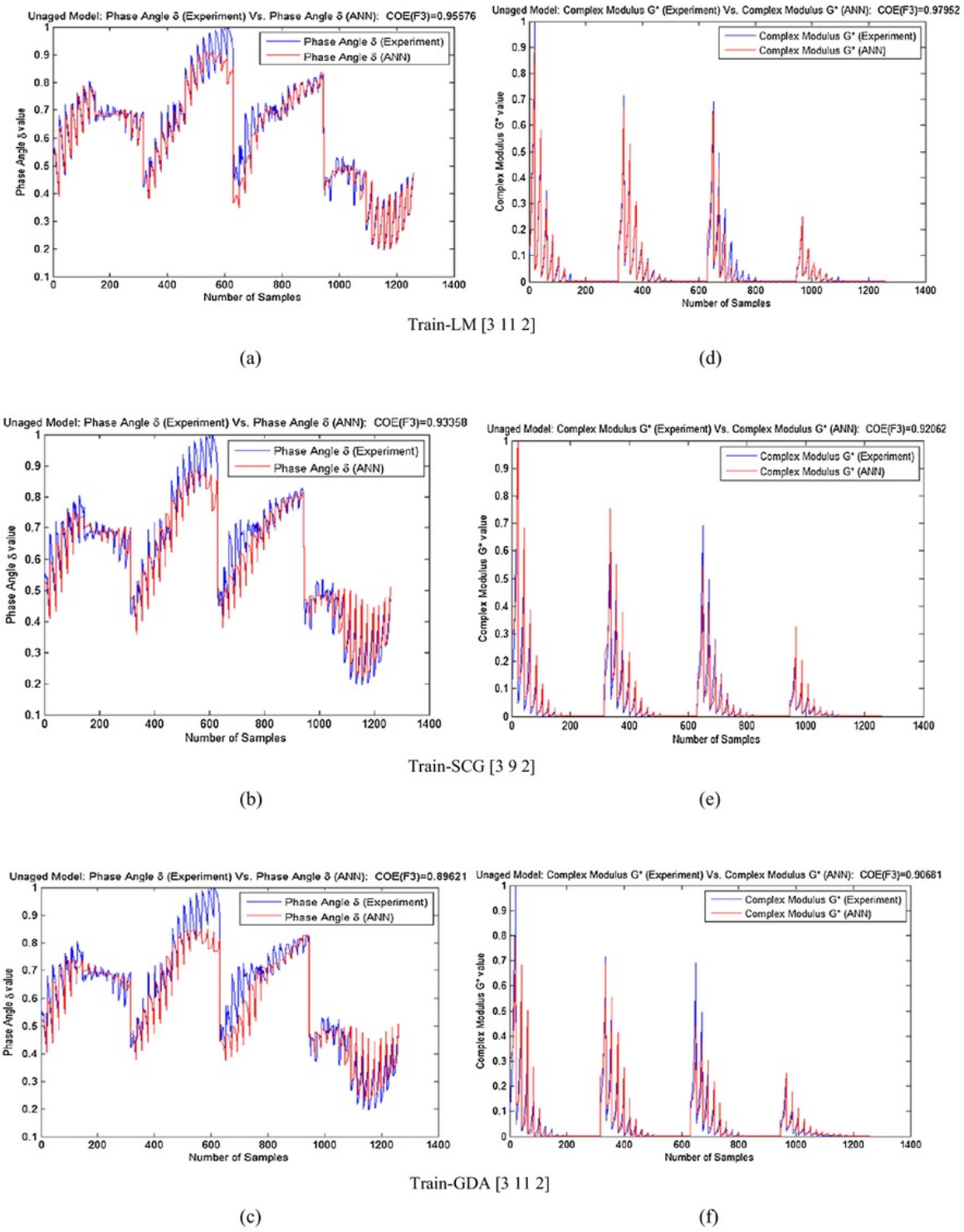

Fig. 11. Performance of ANN-unaged model based on 5-FCV with fold 3 and topology for Train-LM [3 11 2], train-SCG [3 9 2] and train-GDA [3 11 2] for after testing for (a–c) phase angle output, and (d–f) complex modulus output.

ing. Hence, NS-PMB6 could become more viscous and exhibit slow complex modulus at high temperatures subsequent to the ageing process.

The master curves for the phase angle were plotted utilising the shift factors obtained from the complex modulus master curves. The phase angle master curves for the aged PMB and NS-PMB6 bin-

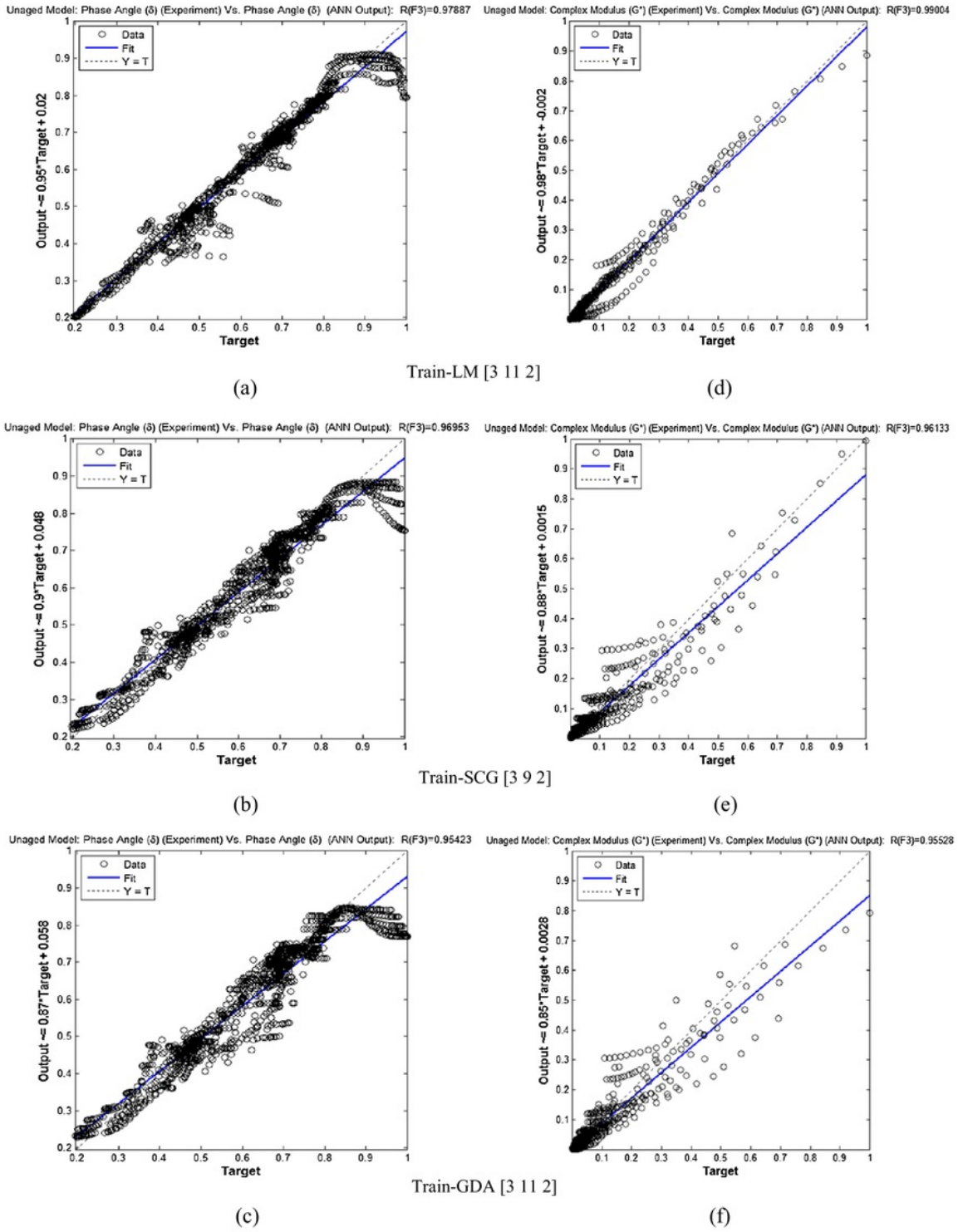

Fig. 12. Regression plot for the testing of ANN-unaged model based 5-FCV with fold 3 and topology for Train-LM [3 11 2], train-SCG [3 9 2] and train-GDA [3 11 2] for (a–c) phase angle, and (d–f) complex modulus.

ders are shown in Figs. 9 and 10, respectively. The phase angle master curve for NS-PMB6 shows that there is an increase in phase angle after the ageing process. These results are identical to those obtained and illustrated in the complex modulus master curve. It summary, the addition of NS particles is able to reduce the effects of ageing on PMB.

3.6. ANN-Unaged model

3.6.1. Training stage

The training process for the neural network is stopped only when the MSE falls below 0.0001 and the neural network have an architecture of [3 5 2], [3 7 2], [3 9 2] and [3 11 2] with three different algorithms, i.e. train-LM, train-SCG and train-GDA, examined in all trials. Table 7 shows the execution to optimise the best ANN design for modelling two outputs.

As can be seen, the models were trained using different training algorithm with differ[19]number of nodes in the hidden layer. Fold three (F3) uses three neurons in the input layer, eleven neurons in the hidden layer, and two neurons in the output layer by using train-LM as the training algorithm (shown in bold type) to produce the best ANN-unaged model. This topology results in the values of MSE, R and COE of 0.0017666, 0.99442, and 0.98888 respectively for the δ as the first output, and MSE, R and COE values of 0.0080262, 0.99728, and 0.99444 respectively for the complex modulus as the second output.

3.6.2. Testing stage

During the testing stage, results are generated and analysed using the best ANN-unaged models obtained from the training stage. In order to test and validate the ANN-unaged model, the output for statistical tests based on MSE, R and the COE were examined between the measured (experiment) and estimated (ANN) outputs. As can be seen in Table 8, a good agreement was obtained for all algorithms in the ANN-unaged model with F3. The results for several simulations show that the best testing performance was obtained for the ANN-unaged model based on the statistical test where COE = 0.95576, MSE = 0.038406, and R = 0.97887 for the first output, δ, and COE = 0.97952, MSE = 0.015655, and R = 0.99004 for the second output, G^*, for the ANN-unaged model based on 5-FCV F3 and topology train-LM [3 11 2].

Here a total of 1,260 samples of the entire training/testing, the ANN-unaged model based 5-FCV F3 and learning algorithm train-LM, train-SCG and train-GDA, were tested based on one hidden layer with varying number neurons, i.e.11, 9 and 11. A curve of laboratory measured and ANN estimated outputs from the testing stage of the ANN decision system were plotted. The curve shows the degree to which a decision system data points match the measured and estimated outputs in decreasing probability. Fig. 11(a–f) shows the graphs of the phase angle and complex modulus experimental data versus the ANN estimated data performed using the 5-FCV based on fold three F3 with three learning algorithm train-LM, train-SCG and train-GDA, respectively. As shown in Fig. 11(a and d), the ANN-unaged model based on 5-FCV with F3 and topology train-LM [3 11 2] produced the best ANN-unaged model based on the performance of 5-FCV which resulted in higher COE and R and lower MSE compared to other folds.

The R plots for testing ANN-unaged models are shown in Fig. 12 (a–f). The plots show that the testing data points for F3 with train-LM [3 11 2] topology falls on the best fit line. This best fit line matched the dotted perfect line, which is hidden in this case due to this matching. In other word, train-LM [3 11 2] topology achieved a testing R value greater than 0.97 for phase angle and 0.99 for complex modulus.

Table 9
Statistical measure from the5-FCV training stage of fold 2with various learning algorithms simulation between measured and examined RTFOT data.

KFCV Learning Algorithms	RTFOT Data: 5-KCV Training Stage with Fold (F = 2)					
	Output 1: Phase angle			**Output 2:** Complex modulus		
	RMSE	R	COE	MSE	R	COE
LM [3–11–2]	0.016863	0.99162	0.98332	0.0080695	0.99668	0.99322
LM [3–9–2]	0.028885	0.97522	0.95105	0.018641	0.98207	0.96438
LM [3–7–2]	0.022028	0.98566	0.97153	0.010862	0.99397	0.98791
LM [3–5–2]	**0.030744**	**0.97188**	**0.94454**	**0.022113**	**0.97466**	**0.94987**
SCG [3–11–2] *	**0.03164**	**0.97019**	**0.94126**	**0.021429**	**0.97621**	**0.95293**
SCG [3–9–2]	0.026436	0.97929	0.959	0.016728	0.98568	0.97132
SCG [3–7–2]	0.03523	0.9629	0.92718	0.019679	0.98007	0.9603
SCG [3–5–2]	0.035968	0.9613	0.9241	0.02516	0.96704	0.93511
GDA [3–11–2]	**0.048742**	**0.92788**	**0.86061**	**0.035579**	**0.93346**	**0.87023**
GDA [3–9–2]	0.04832	0.92912	0.86301	0.038958	0.91976	0.84442
GDA [3–7–2]	0.042388	0.94599	0.89459	0.039647	0.9168	0.83887
GDA [3–5–2]	0.040256	0.9514	0.90492	0.032076	0.94654	0.89453

The bold values are shows the best model for different learning algorithms during training and testing stage.

Table 10
Statistical measure from the5-FCV testing stage of fold 2 with various learning algorithms simulation between measured and examined RTFOT data.

KFCV Learning Algorithms	RTFOT Data: 5-KCV Testing Stage with Fold (F = 2)					
	Output 1: Phase angle			**Output 2:** Complex modulus		
	MSE	R	COE	MSE	R	COE
LM [3–11–2]	0.052448	0.91992	0.83878	0.071192	0.81348	0.656
LM [3–9–2]	0.043649	0.94333	0.88834	0.096639	0.66491	0.36613
LM [3–7–2]	0.036407	0.9619	0.92232	0.078892	0.8132	0.57757
LM [3–5–2]	**0.038547**	**0.95741**	**0.91292**	**0.072038**	**0.81763**	**0.64778**
SCG [3–11–2] *	**0.034124**	**0.96534**	**0.93176**	**0.03504**	**0.95862**	**0.91667**
SCG [3–9–2]	0.051037	0.92332	0.84735	0.068909	0.82643	0.67771
SCG [3–7–2]	0.045113	0.94374	0.88073	0.056186	0.89771	0.78574
SCG [3–5–2]	0.042682	0.94539	0.89324	0.051447	0.91287	0.82036
GDA [3–11–2]	**0.053162**	**0.91576**	**0.83437**	**0.062319**	**0.8839**	**0.7364**
GDA [3–9–2]	0.062054	0.88387	0.77433	0.068313	0.84482	0.68326
GDA [3–7–2]	0.081549	0.80183	0.61026	0.056815	0.89917	0.78091
GDA [3–5–2]	0.052415	0.9165	0.83899	0.07365	0.80873	0.63184

The bold values are shows the best model for different learning algorithms during training and testing stage.

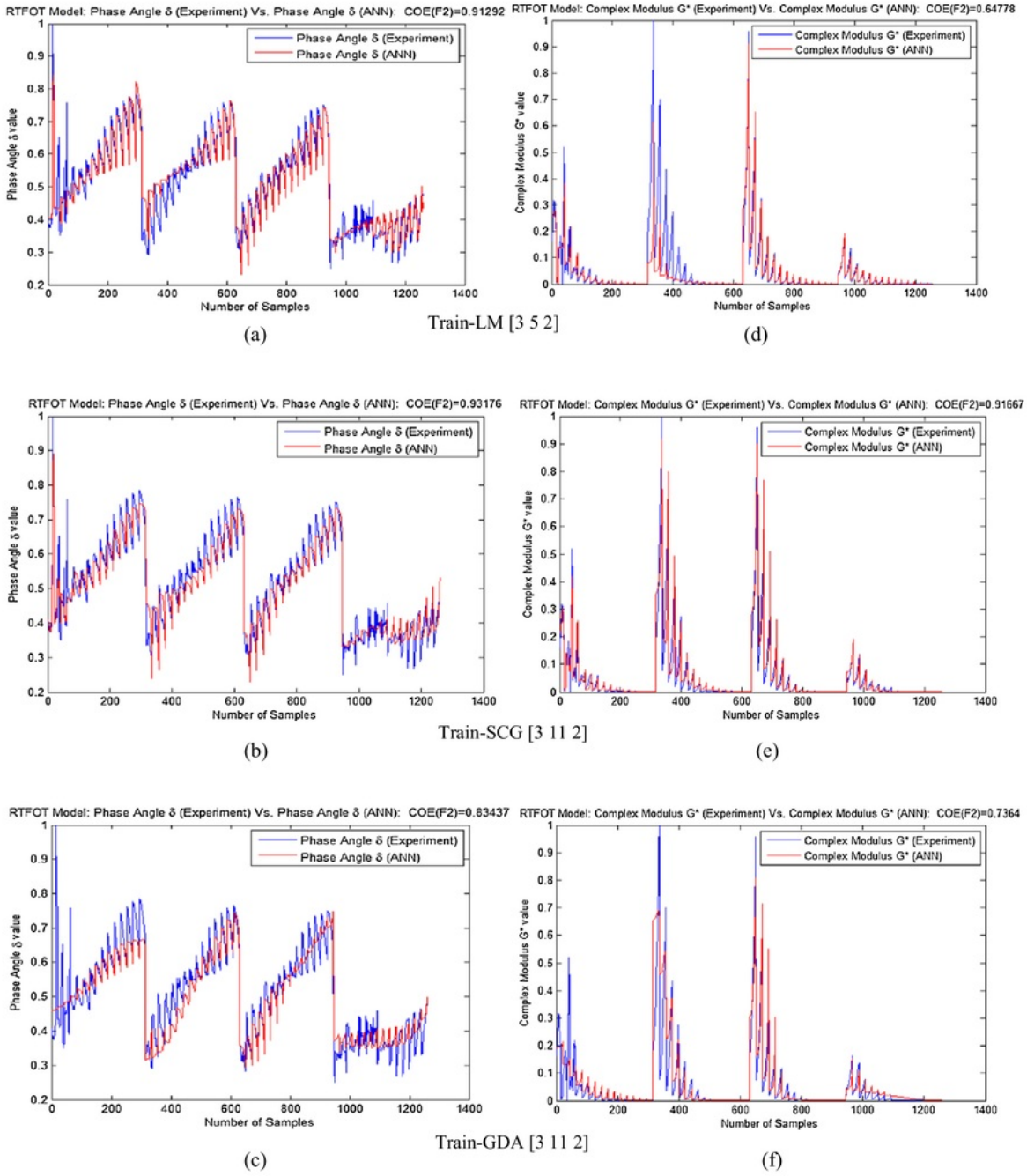

Fig. 13. Performance of ANN-RTFOT model based on 5-FCV with fold 2 and topology for Train-LM [3 5 2], Train-SCG [3 11 2] and Train-GDA [3 11 2] after testing for (a–c) phase angle output, and (d–f) complex modulus output.

3.7. ANN-RTFOT model

3.7.1. Training stage

For the RTFOT data training, various ANN topologies based on varying numbers of hidden layer neurons are examined by utilising the statistical weighting pre-processed inputs. The statistical measures involved are MSE, R and COE. Accuracy could be improved by analysing the results of this training results; this is done through different learning algorithms, i.e. train-LM, train-SCG and train-GDA, and by varying the number of hidden neurons as indicated by smaller MSE and values approaching 1 for R and COE. The analysis of statistical measures obtained in the ANN-RTFOT models based on 5-FCV with fold two (F2) is given in Table 9; it shows that the SCG algorithm yields excellent performance compared to the LM and GDA algorithms. Amongst the SCG algorithms, the train-SCG [3 11 2] structure algorithm produced the most optimal topology. For the phase angle, which represent the first input, the RMSE, R and COE topology values are 0.03164, 0.97019 and 0.94126

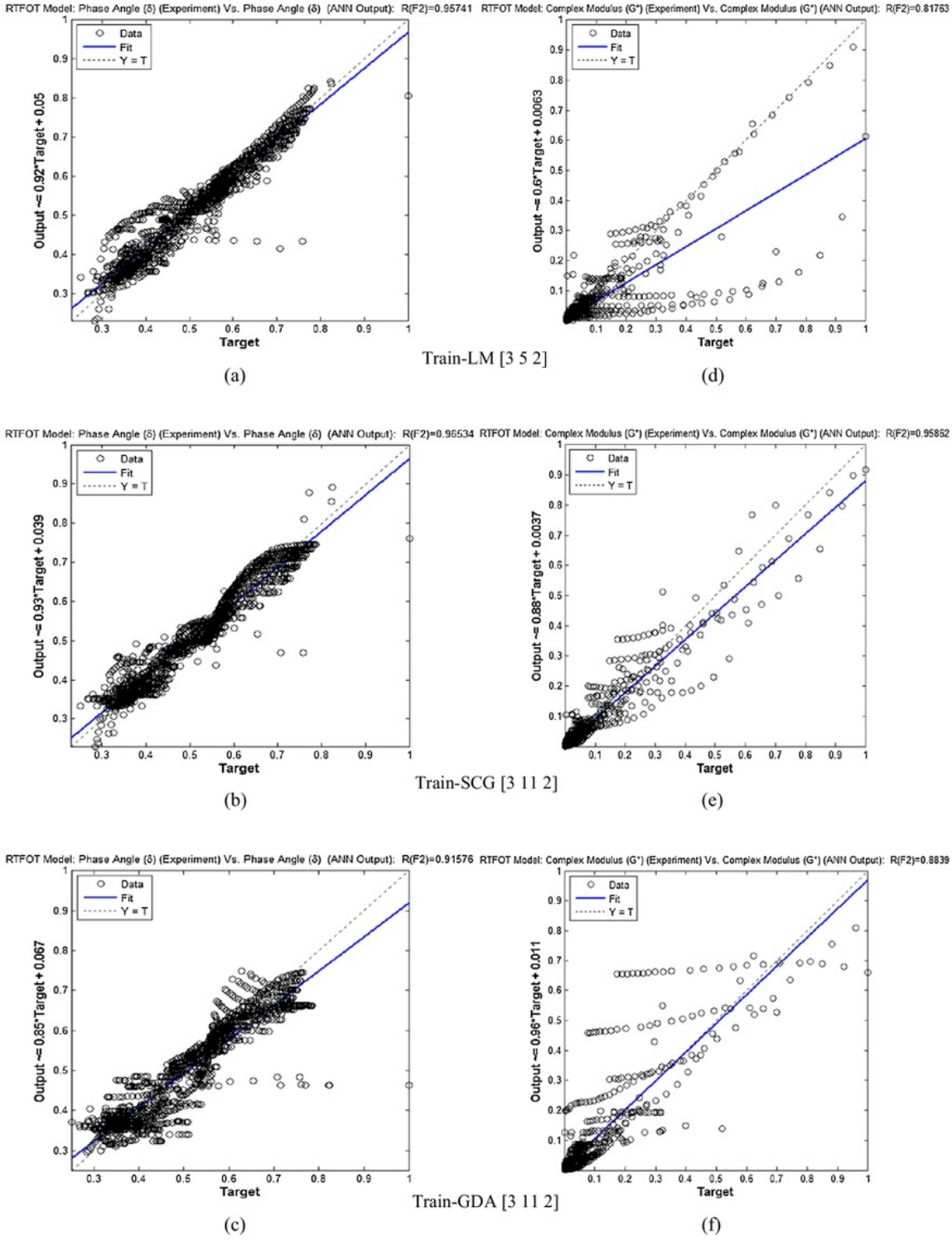

Fig. 14. Regression plot for the testing of ANN-RTFOT model based on 5-FCV with fold 2 and topology for Train-LM [3 5 2], Train-SCG [3 11 2] and Train-GDA [3 11 2] for (a–c) phase angle and (d–f) complex modulus.

respectively, while the values for the complex modulus as the second output are 0.021429, 0.97621, and 0.95293 respectively.

3.7.2. Testing stage

In the RTFOT data testing stage, results were generated and analysed using the best ANN-RTFOT models obtained from the training stage. Analysis of the data points which gives the MSE, R and COE values for the ANN-RTFOT model was examined for the measured (experiment) and estimated (ANN) outputs. To assess the performance of the phase angle and complex modulus prediction, the entire dataset was checked in the testing stage. The prediction of performance based on the 5-FCV to the model RTFOT dataset have topologies of train-LM [3 5 2], train-SCG [3 11 2] and train-GDA [3 11 2] at all trails. The results for several simulations show that the best testing performance was obtained for the ANN-RTFOT model based on the statistical test where COE = 0.93176, MSE = 0.034124, and R = 0.96534 for the first output, phase angle, and COE = 0.91667, MSE = 0.03504, and R = 0.95862 for the second output, complex modulus, for the ANN-RTFOT model based on 5-FCV F2 and topology train-SCG [3 11 2]. This result is shown in Table 10.

In view of the second instance of testing examination, the ANN-RTFOT model based on 5-FCV with F2 and learning algorithm train-LM, train-SCG and train-GDA, separately are approved based various neurons of 5, 11 and 11 on single hidden layer. A laboratory measured and ANN estimated outputs curve from the testing stage of the ANN-RTFOT decision system was also examined. Fig. 13(a–f) shows the best results obtained from experimental data versus the ANN estimated data from five trials which used three the different algorithms (train-LM, train-SCG and train-GDA) for ANN-RTFOT model based on 5-FCV with F2. The curve shows the degree to which the decision system data points match the measured and estimated output in order of decreasing probability. Fig. 13(b and e) shows the graphs for δ and G^* experimental data versus ANN estimated data plotted using the 5-FCV based on F2 with the most optimal topology, i.e. train-SCG [3 11 2].

The R plots for ANN-RTFOT testing are shown in Fig. 14(a–f). It can be noted from the R plots that the testing which produced higher R values were in F2 with train-SCG [3 11 2], which resulted in a recorded 0.96534 for phase angle and 0.95862 for complex modulus.

3.8. ANN-PAV model

3.8.1. Training stage

In this stage, the same protocol for ANN topologies training investigations was adopted for varying number of hidden layer neurons. The results for statistical measurement of MSE, R and COE are presented in Table 11.

Results with smaller MSE and higher R and COE values approaching 1 indicate that training accuracy is enhanced by different learning algorithms, i.e. train-LM, train-SCG, and train-GDA, and by changing the number of hidden neurons. From the statistical measures obtained in the ANN-PAV model based on 5-FCV with fold 3 and train-LM algorithm yields results which are compared to the SCG and GDA algorithms. Amongst the train-LM

Table 11
Statistical measures from the 5-FCV training stage of fold 3with various learning algorithms simulation between measured and examined PAV data.

KFCV Learning Algorithms	PAV Data: 5-FCV Training Stage with Fold (F = 3)					
	Output 1: Phase angle			**Output 2:** Complex modulus		
	MSE	R	COE	MSE	R	COE
LM [3–11–2]	0.016209	0.99533	0.99069	0.0057423	0.99867	0.99734
LM [3–9–2] *	**0.018694**	**0.99379**	**0.98761**	**0.0059808**	**0.99856**	**0.99711**
LM [3–7–2]	0.018674	0.9938	0.98764	0.0088373	0.99691	0.99369
LM [3–5–2]	0.028679	0.98532	0.97084	0.016335	0.98953	0.97844
SCG [3–11–2]	0.035315	0.97772	0.95579	0.019105	0.98536	0.97051
SCG [3–9–2]	**0.020456**	**0.99256**	**0.98517**	**0.011102**	**0.99519**	**0.99004**
SCG [3–7–2]	0.019311	0.99337	0.98678	0.0087053	0.99701	0.99388
SCG [3–5–2]	0.020794	0.99231	0.98467	0.010185	0.99592	0.99165
GDA [3–11–2]	0.03254	0.98113	0.96246	0.031055	0.96125	0.92208
GDA [3–9–2]	0.030117	0.98382	0.96784	0.028683	0.96652	0.93353
GDA [3–7–2]	**0.038396**	**0.97361**	**0.94774**	**0.03271**	**0.95671**	**0.91355**
GDA [3–5–2]	0.032583	0.98103	0.96236	0.028515	0.96687	0.9343

The bold values are shows the best model for different learning algorithms during training and testing stage.

Table 12
Statistical measure from the 5-FCV testing stage of fold 3 with various learning algorithms simulation between measured and examined PAV data.

KFCV Learning Algorithms	PAV Data: 5-KCV Testing Stage with Fold (F = 3)					
	Output 1: Phase angle			**Output 2:** Complex modulus		
	MSE	R	COE	MSE	R	COE
LM [3–11–2]	0.018643	0.99418	0.98799	0.026374	0.97744	0.94946
LM [3–9–2] *	**0.020478**	**0.99298**	**0.98551**	**0.025344**	**0.97942**	**0.95333**
LM [3–7–2]	0.031169	0.98332	0.96644	0.069343	0.81763	0.6506
LM [3–5–2]	0.031065	0.98358	0.96667	0.039196	0.94943	0.88837
SCG [3–11–2]	0.034766	0.97901	0.95825	0.044512	0.93108	0.85603
SCG [3–9–2]	**0.021863**	**0.99182**	**0.98349**	**0.035557**	**0.95942**	**0.90813**
SCG [3–7–2]	0.036434	0.97759	0.95415	0.040548	0.94372	0.88053
SCG [3–5–2]	0.028568	0.98642	0.97181	0.050819	0.90762	0.81234
GDA [3–11–2]	0.035378	0.9782	0.95677	0.04486	0.92887	0.85377
GDA [3–9–2]	0.032938	0.98167	0.96252	0.057018	0.88065	0.76377
GDA [3–7–2]	**0.038822**	**0.97376**	**0.94794**	**0.039073**	**0.94738**	**0.88907**
GDA [3–5–2]	0.036115	0.97749	0.95495	0.047353	0.92102	0.83707

The bold values are shows the best model for different learning algorithms during training and testing stage.

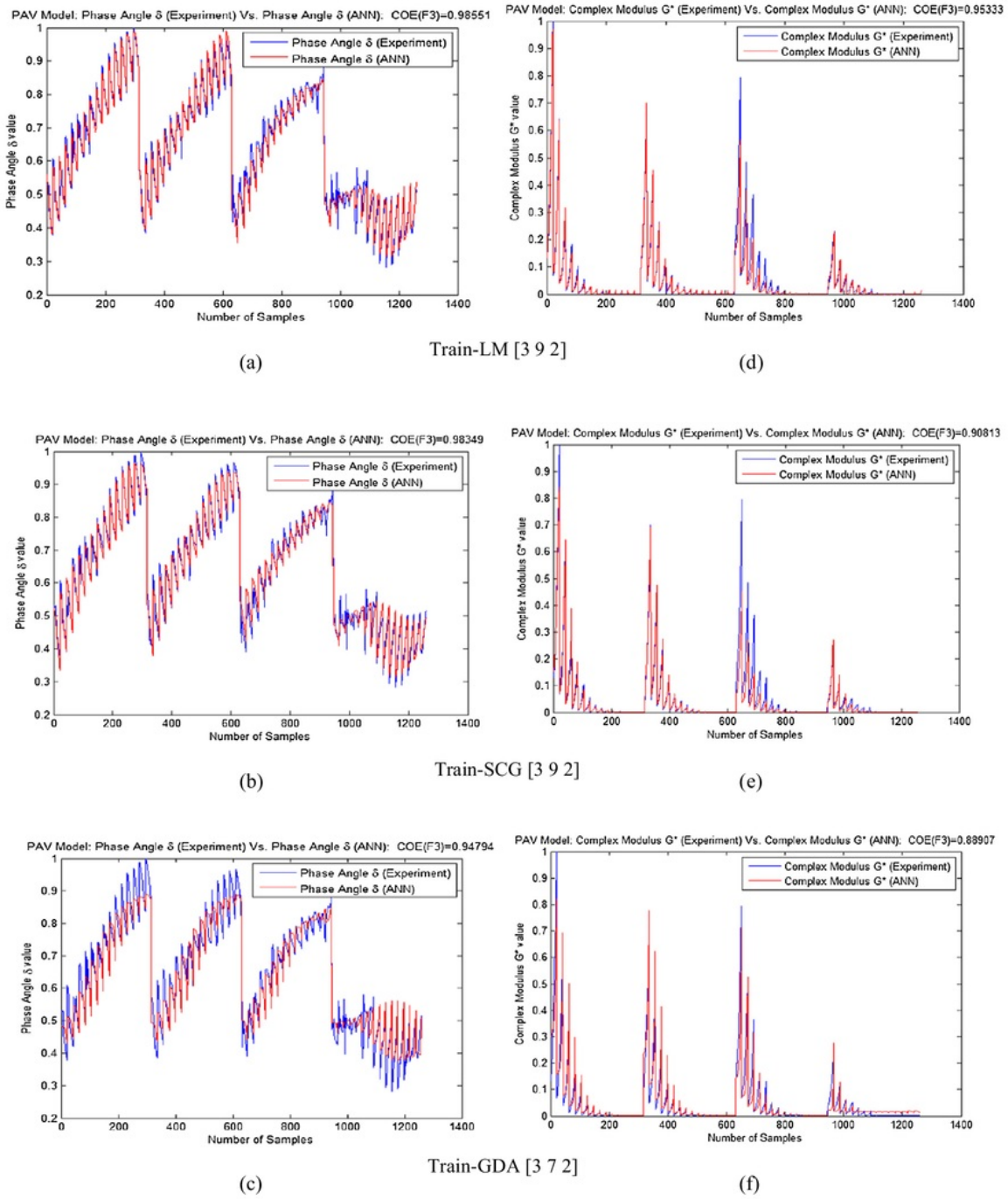

Fig. 15. Performance of ANN-PAV model based on 5-FCV with fold 3 and topology for Train-LM [3 9 2], Train-SCG [3 8 2] and Train-GDA [3 7 2] for after testing for (a–c) phase angle output, and (d–f) complex modulus output.

algorithm, the train-LM [3 9 2] topology algorithm produced the most optimal topology. For the phase angle which represents the first input, the values for MSE, R and COE topology are 0.018694, 0.99379 and 0.98761 respectively, while the values of MSE, R and COE for the complex modulus as the second output are 0.0059808, 0.99856, and 0.99711 respectively.

3.8.2. Testing stage

In the PAV data testing stage, results were generated and analysed using the selected model in the training stage. The analysed data points produced the MSE, R and COE for the ANN-PAV model for predicting the accuracy of the testing data. To assess the performance of the phase angle and the complex modulus prediction, the

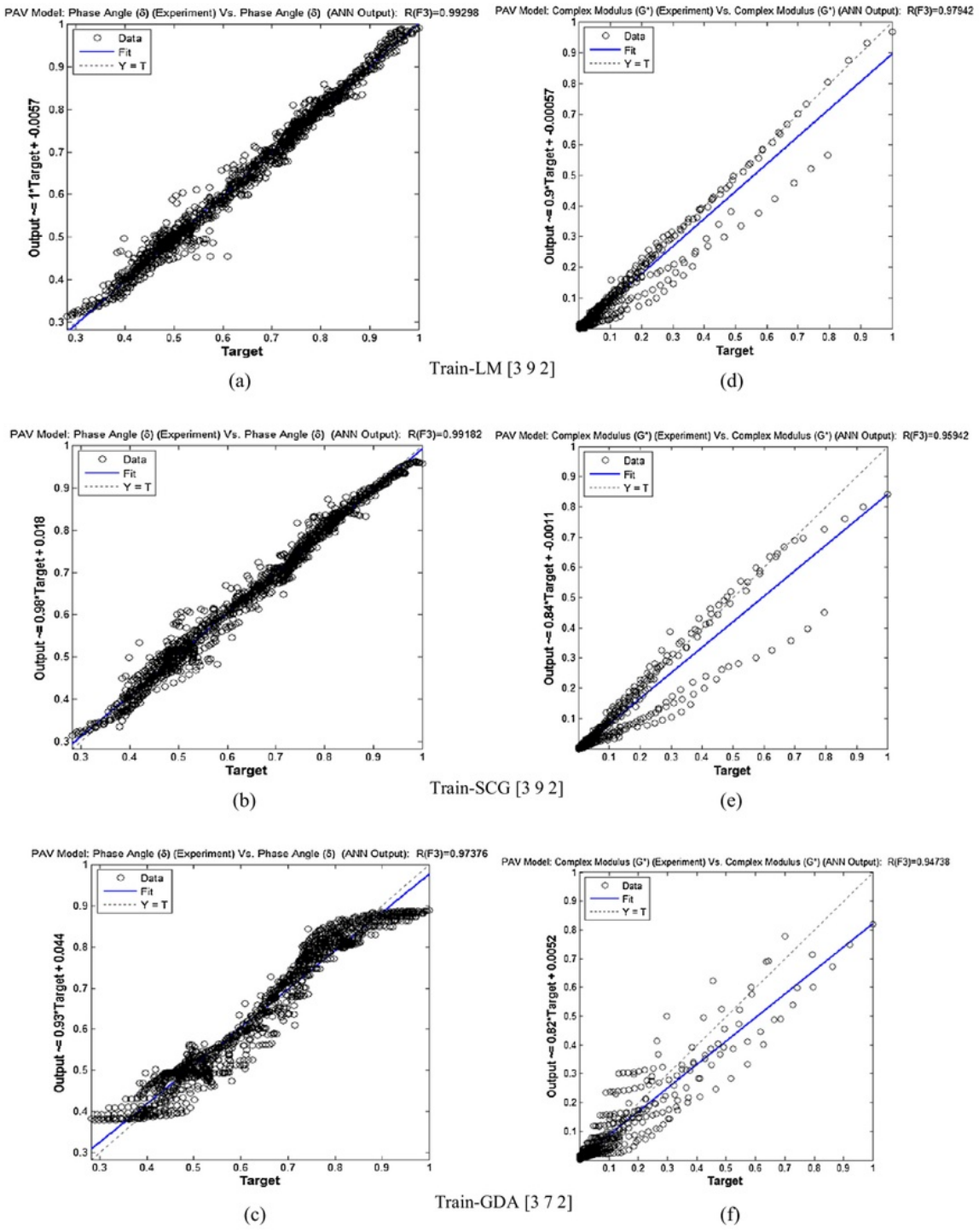

Fig. 16. Regression plot for the testing of ANN-PAV model based on 5-FCV with fold 3 and topology for Train-LM [3 9 2], Train-SCG [3 8 2] and Train-GDA [3 7 2] for after testing for (a–c) phase angle, and (d–f) complex modulus.

entire dataset was checked in the testing stage. The performance prediction based on the 5-FCV to model the PAV dataset have topologies train-LM [3 9 2], Train-SCG [3 9 2] and train-GDA [3 7 2] at all trails. The results for several simulations show that the best testing performance was obtained for the ANN-PAV model based on the statistical test where COE = 0.98551, MSE = 0.020478,

and R = 0.99298 for the first output, phase angle, and COE = 0.95333, MSE = 0.025344, and R = 0.97942 for the second output, complex modulus, for the ANN-PAV model based on 5-FCV F3 and topology train-LM [3 9 2]. This result is shown in Table 12.

In view of the second instance of testing examination, the ANN-PAV model based on 5-FCV with F3 and learning algorithm train-LM, train-SCG and train-GDA, separately are approved based various neurons of 9, 9 and 7 on single hidden layer. A laboratory measured and ANN estimated outputs curve from the testing stage of the ANN-PAV decision system was also examined. Fig. 15(a–f) shows the best results obtained from the experimental data versus the ANN estimated data from the five trials using the three different algorithms (train-LM, train-SCG and train-GDA) for the ANN-PAV model based on 5-FCV with F3. The curve shows the degree to which a decision system data points match the measured and estimated outputs in order of decreasing probability. Fig. 15(a and d) shows the graphs of the δ and G* experimental data versus the ANN estimated data performed by the 5-FCV based on F3 with the best optimal topology of train-LM [3 9 2].

The R plots for the testing of ANN-PAV models shown in Fig. 16 (a–f) provide more evidence for matching by recording the R values during testing. In other words, ANN-PAV in F3 with train-LM [3 9 2] topology achieved a testing R value greater than 0.99 for phase angle and 0.97 for complex modulus. The scattering in the R plots for F3 with train-LM [3 9 2] of both outputs are less than other topologies in F3. It can be seen that the testing data points are located on the best fit line.

4. Conclusions

Based on the outcome of this study, the following conclusions can be drawn:

- The results of the FTIR show an increase in the carbonyl index of the NS-PMB binder. This indicates that the addition of NS to PMB could weaken and delay the ageing process of bituminous binders. On the other hand, the results for the X-RD shows that the amorphous structures of NS-PMBs remain unchanged and no new crystalline phase was formed when varying percentages of NS was added to PMB. Morphological analysis showed a change in the microstructure of NS-PMBs binders and a good dispersion of NS particles in PMB was observed.
- Overall, high temperatures significantly increased the complex modulus of NS-PMB6 while low temperatures reduced the binder's complex modulus. This has resulted in improved resistance to rutting and fatigue parameters. Likewise, adding higher amounts of NS particles to PMB improve the viscoelastic properties of NS-PMB6 as the complex modulus increase at high temperatures and/or low frequencies and decrease at low temperatures and/or high frequencies. In summary, NS-PMBs show good resistance to the ageing conditions.
- The best algorithm to predict the phase angle and complex modulus for unaged NS-PMBs sample is LM algorithm. The proposed ANN models for phase angle and complex modulus have shown good agreement to the experimental result with R value is 0.978 and 0.990 respectively. The most suitable neuron number in the hidden layer for this model is 11 neurons. For unaged sample, the MSE and COV value were determined as 0.038 and 0.016 respectively for phase angle and 0.016 and 0.980 respectively for complex modulus.
- For the ANN-RTFOT model to predict the phase angle and complex modulus for short term aging NS-PMBs the best algorithm is SCG algorithm and the optimum number of neuron in the hidden layer is 11. The R value for this model is 0.965 for phase angle and 0.959 for complex modulus indicating the best agreement to the experimental result. The MSE and COV value was reported as 0.034 and 0.932 accordingly for phase angle and 0.035 and 0.917 respectively for complex modulus.
- The prediction of phase angle and complex modulus for long term aging NS-PMBs was conducted using ANN-PAV model. This model indicated that the best algorithm is LM and the most suitable number of neuron in the hidden layer is 9. The correlation between prediction and the experimental result shown high with R value is 0.993 and 0.979, both for prediction of phase angle and complex modulus. The MSE and COV value was determined as 0.020 and 0.986 for phase angle and 0.025 and 0.953 for complex modulus.

Acknowledgements

The authors would like to express their gratitude to Universiti Kebangsaan Malaysia (UKM) for the financial support for this work (DIP-2017-004).

Conflicts of interest statement

The Authors declare that there is no conflict of interest regarding the publication of this paper.

References

[1] X. Lu, Polymer modified road bitumens, Royal Inst. of Tech., Dept. of Infrastructure and Planning, Stockholm, Sweden, 1997.
[2] G. Airey, Styrene butadiene styrene polymer modification of road bitumens, J. Mater. Sci. 39 (3) (2004) 951–959, https://doi.org/10.1023/B:JMSC.0000012927.00747.83.
[3] C. Giavarini et al., Production of stable polypropylene-modified bitumens, Fuel 75 (6) (1996) 681–686.
[4] M. Panda, M. Mazumdar, Engineering properties of EVA-modified bitumen binder for paving mixes, J. Mater. Civ. Eng. 11 (2) (1999) 131–137.
[5] G. Polacco et al., Asphalt modification with different polyethylene-based polymers, Eur. Polym. J. 41 (12) (2005) 2831–2844.
[6] R.K. Padhan, A.A. Gupta, Preparation and evaluation of waste PET derived polyurethane polymer-modified bitumen through in situ polymerization reaction, Constr. Build. Mater. 158 (2018) 337–345.
[7] B. Sengoz, A. Topal, G. Isikyakar, Morphology and image analysis of polymer modified bitumens, Constr. Build. Mater. 23 (5) (2009) 1986–1992.
[8] M. Çalışıcı, M. Gürü, M.K. Çubuk, Ö.F. Cansız, Improving the aging resistance of bitumen by addition of polymer-based diethylene glycol, Constr. Build. Mater. 169 (2018) 283–288.
[9] S. Tayfur, H. Ozen, A. Aksoy, Investigation of rutting performance of asphalt mixtures containing polymer modifiers, Constr. Build. Mater. 21 (2) (2007) 328–337.
[10] C. Gorkem, B. Sengoz, Predicting stripping and moisture induced damage of asphalt concrete prepared with polymer modified bitumen and hydrated lime, Constr. Build. Mater. 23 (6) (2009) 2227–2236.
[11] T. Alataş, M. Yilmaz, Effects of different polymers on mechanical properties of bituminous binders and hot mixtures, Constr. Build. Mater. 42 (2013) 161–167, https://doi.org/10.1016/j.conbuildmat.2013.01.027.
[12] J. Zhu, B. Birgisson, N. Kringos, Polymer modification of bitumen: advances and challenges, Eur. Polym. J. 54 (2014) 18–38.
[13] F. Xiao, A.N. Amirkhanian, S.N. Amirkhanian, Influence of carbon nanoparticles on the rheological characteristics of short-term aged asphalt binders, J. Mater. Civ. Eng. 23 (4) (2010) 423–431.
[14] J. Cheng, J. Shen, F. Xiao, Moisture susceptibility of warm-mix asphalt mixtures containing nanosized hydrated lime, J. Mater. Civ. Eng. 23 (11) (2011) 1552–1559, https://doi.org/10.1061/(ASCE)MT.1943-5533.0000308.
[15] Z. You et al., Nanoclay-modified asphalt materials: Preparation and characterization, Constr. Build. Mater. 25 (2) (2011) 1072–1078.
[16] G. Lazzara, S. Milioto, Dispersions of nanosilica in biocompatible copolymers, Polym. Degrad. Stab. 95 (4) (2010) 610–617.
[17] H. Yao et al., Rheological properties and chemical bonding of asphalt modified with nanosilica, J. Mater. Civ. Eng. 25 (11) (2012) 1619–1630.
[18] J. Yang, S. Tighe, A review of advances of nanotechnology in asphalt mixtures, Procedia-Soc. Behav. Sci. 96 (2013) 1269–1276.
[19] H. Ceylan, K. Gopalakrishnan, S. Kim, Advanced approaches to hot-mix asphalt dynamic modulus prediction, Can. J. Civ. Eng. 35 (7) (2008) 699–707.
[20] B.V. Kok, M. Yilmaz, B. Sengoz, A. Sengur, E. Avci, Investigation of complex modulus of base and SBS modified bitumen with artificial neural networks, Expert Syst. Appl. 37 (12) (2010) 7775–7780.

[21] ASTM-D36, American Society for Testing and Materials, Standard Test Method for Softening Point of Bitumen (Ring-and-Ball Apparatus), Conshohocken, Pennsylvania, USA, 1995.
[22] ASTM-D5, American Society for Testing and Materials, Standard Test Method for Penetration of Bituminous Materials, Conshohocken, Pennsylvania, USA, 1997.
[23] ASTM D4402, Standard Test Method for Viscosity Determinations of Unfilled Asphalts Using the Brookfield Thermosel Apparatus, American Society for Testing and Materials, Conshohocken, Pennsylvania, USA, 2000.
[24] ASTM-D113, American Society for Testing and Materials, Standard Test Method for Ductility of Bituminous Materials, Conshohocken, Pennsylvania, USA, 1999.
[25] ASTM D2872, American Society for Testing and Materials, Standard Test Method for Effect of Heat and Air on a Moving Film of Asphalt (Rolling Thin-Film Oven Test), Conshohocken, Pennsylvania, USA, 2012.
[26] ASTM D6521, American Society for Testing and Materials, Standard Practice for Accelerated Aging of Asphalt Binder Using a Pressurized Aging Vessel (PAV), Conshohocken, Pennsylvania, USA, 2005.
[27] W.J. Deng, W.C. Chen, W. Pei, Back-propagation neural network based importance performance analysis for determining critical service attributes, Expert Syst. Appl. 34 (2) (2008) 1115–1125.
[28] H.B. Demuth, M.H. Beale, O. De Jess, M.T. Hagan, Neural network design, Martin Hagan, 2014.
[29] H. Adib, R. Haghbakhsh, M. Saidi, M.A. Takassi, F. Sharifi, M. Koolivand, M.R. Rahimpour, S. Keshtkari, Modeling and optimization of Fischer Tropsch synthesis in the presence of Co (III)/Al_2O_3 catalyst using artificial neural networks and genetic algorithm, J. Nat. Gas Sci. Eng. 10 (2013) 14–24.
[30] A. Mustapha, A. Hussain, S.A. Samad, M.A. Zulkiey, Toward under-specified queries enhancement using retrieval and classification platforms, Computational Intelligence for Multimedia, Signal and Vision Processing (CIMSIVP), 2014, IEEE Symposium on 1–7.
[31] M. Cortizo et al., Effect of the thermal degradation of SBS copolymers during the ageing of modified asphalts, Polym. Degrad. Stab. 86 (2) (2004) 275–282.
[32] D.O. Larsen et al., Micro-structural and rheological characteristics of SBS-asphalt blends during their manufacturing, Constr. Build. Mater. 23 (8) (2009) 2769–2774.
[33] C. Ouyang et al., Improving the aging resistance of styrene–butadiene–styrene tri-block copolymer modified asphalt by addition of antioxidants, Polym. Degrad. Stab. 91 (4) (2006) 795–804.
[34] F. Zhang, J. Yu, J. Han, Effects of thermal oxidative ageing on dynamic viscosity, TG/DTG, DTA and FTIR of SBS-and SBS/sulfur-modified asphalts, Constr. Build. Mater. 25 (1) (2011) 129–137.
[35] S.I.A. Ali et al., Performance evaluation of Al_2O_3 nanoparticle-modified asphalt binder, Road Mater. Pavement Des. (2016) 1–18, https://doi.org/10.1080/14680629.2016.1208621.

[J] CBM_Eng Characteristics_Q1_2019

ORIGINALITY REPORT

8%	%	8%	%
SIMILARITY INDEX	INTERNET SOURCES	PUBLICATIONS	STUDENT PAPERS

PRIMARY SOURCES

1	Yao, Hui, Zhanping You, Liang Li, Shu Wei Goh, Chee Huei Lee, Yoke Khin Yap, and Xianming Shi. "Rheological properties and chemical analysis of nanoclay and carbon microfiber modified asphalt with Fourier transform infrared spectroscopy", Construction and Building Materials, 2013. Publication	1%
2	Yao, Hui, Zhanping You, Liang Li, Chee Huei Lee, David Wingard, Yoke Khin Yap, Xianming Shi, and Shu Wei Goh. "Rheological Properties and Chemical Bonding of Asphalt Modified with Nanosilica", Journal of Materials in Civil Engineering, 2013. Publication	1%
3	Hasan Taherkhani, Siamark Afroozi. "Investigating the creep properties of asphaltic concrete containing nano-silica", Sādhanā, 2018 Publication	<1%
	Ozgoren, M.. "Estimation of global solar	

4	radiation using ANN over Turkey", Expert Systems With Applications, 201204 Publication	<1%
5	Habibullah Akbar, Nanna Suryana, Shahrin Sahib. "Training neural networks using Clonal Selection Algorithm and Particle Swarm Optimization: A comparisons for 3D object recognition", 2011 11th International Conference on Hybrid Intelligent Systems (HIS), 2011 Publication	<1%
6	Gordon D. Airey. "Rheological evaluation of ethylene vinyl acetate polymer modified bitumens", Construction and Building Materials, 2002 Publication	<1%
7	"Testing and Characterization of Sustainable Innovative Bituminous Materials and Systems", Springer Science and Business Media LLC, 2018 Publication	<1%
8	"8th RILEM International Conference on Mechanisms of Cracking and Debonding in Pavements", Springer Science and Business Media LLC, 2016 Publication	<1%
9	"Investigation on the physical and rheological	

properties of acrylate-styrene-acrylonitrile polymer and nano aluminum oxide modified asphalt binders nano aluminum oxide modified asphalt binders", Bituminous Mixtures and Pavements VI, 2015.
Publication

<1%

---

10 Marzieh Habibi Karahrodi, Omid Moini Jazani, Seyed Mohammad Reza Paran, Krzysztof Formela, Mohammad Reza Saeb. "Modification of thermal and rheological characteristics of bitumen by waste PET/GTR blends", Construction and Building Materials, 2017
Publication

<1%

---

11 Airey, G.D.. "Rheology of polyacrylate binders produced via catalytic chain transfer polymerization as an alternative to bitumen in road pavement materials", European Polymer Journal, 201106
Publication

<1%

---

12 Xie, Yanjun, Liantong Mo, Donglin Su, M.F. Woldekidan, and Shaopeng Wu. "Investigation into fundamental properties of bituminous plug expansion joint filling mixtures containing rubber granules", Construction and Building Materials, 2013.
Publication

<1%

---

13 Zuzana Cizkova, Jan Suda. "Viscoelastic

<1%

behaviour of cold recycled asphalt mixes", IOP Conference Series: Materials Science and Engineering, 2017
Publication

---

14 F. Moreno-Navarro, M. Sol-Sánchez, F. Gámiz, M.C. Rubio-Gámez. "Mechanical and thermal properties of graphene modified asphalt binders", Construction and Building Materials, 2018 <1%
Publication

---

15 B. V. Ayodele, M. R. Khan, C. K. Cheng. "Greenhouse gases abatement by catalytic dry reforming of methane to syngas over samarium oxide-supported cobalt catalyst", International Journal of Environmental Science and Technology, 2017 <1%
Publication

---

16 Ramez A. Al-Mansob, Amiruddin Ismail, Riza Atiq O.K. Rahmat, Muhamad Nazri Borhan et al. "The performance of Epoxidised Natural Rubber modified asphalt using nano-alumina as additive", Construction and Building Materials, 2017 <1%
Publication

---

17 Cao Kai, Xu Wenyuan, Chen Dan, Feng Huimin. "High- and Low-Temperature Properties and Thermal Stability of Silica <1%

Fume/SBS Composite-Modified Asphalt Mortar", Advances in Materials Science and Engineering, 2018
Publication

18	Jie Yuan, Jiayu Wang, Feipeng Xiao, Serji Amirkhanian, Jun Wang, Zhizhou Xu. "Impacts of multiple-polymer components on high temperature performance characteristics of airfield modified binders", Construction and Building Materials, 2017 Publication	<1%
19	Deng, W.J.. "Fuzzy neural based importance-performance analysis for determining critical service attributes", Expert Systems With Applications, 200903 Publication	<1%
20	Industrial Lubrication and Tribology, Volume 65, Issue 6 (2013-09-28) Publication	<1%
21	"Polymer Dispersions and Their Industrial Applications", Wiley, 2002 Publication	<1%
22	Lei, Zhang, Li Tian-shuai, Gao Fei, and Tan Yi-qiu. "Rheological and physical properties of asphalt mixed with warm compaction modifier", Construction and Building Materials, 2016. Publication	<1%

23	Diana Gómez-Heincke, Inmaculada Martínez, Mats Stading, Críspulo Gallegos, Pedro Partal. "Improvement of mechanical and water absorption properties of plant protein based bioplastics", Food Hydrocolloids, 2017 Publication	<1%
24	Jia-Jiunn Lo, Pai-Chuan Shu. "Identification of learning styles online by observing learners' browsing behaviour through a neural network", British Journal of Educational Technology, 2004 Publication	<1%
25	Tiğdemir, Mesut. "Re-Evaluation of the AASHTO-Flexible Pavement Design Equation with Neural Network Modeling", PLoS ONE, 2014. Publication	<1%
26	Hossein Nazari, Koorosh Naderi, Fereidoon Moghadas Nejad. "Improving aging resistance and fatigue performance of asphalt binders using inorganic nanoparticles", Construction and Building Materials, 2018 Publication	<1%
27	Desmond Threadingham. "Rubber, 3. Synthetic", Ullmann s Encyclopedia of Industrial Chemistry, 07/31/2003 Publication	<1%

28	Hui Yao, Zhanping You. "Nanoclay modified asphalt", Elsevier BV, 2016 Publication	<1%
29	J.-S. Chen. "How Good Are Linear Viscoelastic Properties of Asphalt Binder to Predict Rutting and Fatigue Cracking?", Journal of Materials Engineering and Performance, 08/01/1999 Publication	<1%
30	Tenn, Nadine, Fatima Allou, Christophe Petit, Joseph Absi, and Sylvie Rossignol. "Formulation of new materials based on geopolymer binders and different road aggregates", Ceramics International, 2015. Publication	<1%
31	Mahmoud Enieb, Aboelkasim Diab. "Characteristics of asphalt binder and mixture containing nanosilica", International Journal of Pavement Research and Technology, 2017 Publication	<1%
32	Feng Zhang, Changbin Hu, Weilong Zhuang. "The research for low-temperature rheological properties and structural characteristics of high-viscosity modified asphalt", Journal of Thermal Analysis and Calorimetry, 2017 Publication	<1%
33	Balasubramanian, S.. "Neural networks-integrated metal oxide-based artificial olfactory	<1%

system for meat spoilage identification", Journal of Food Engineering, 200903
Publication

---

34 Ming Liang, Xue Xin, Weiyu Fan, Hao Wang, Shisong Ren, Jingtao Shi. "Effects of polymerized sulfur on rheological properties, morphology and stability of SBS modified asphalt", Construction and Building Materials, 2017 <1%
Publication

---

35 RUDY SETIONO. "A Neural Network Construction Algorithm which Maximizes the Likelihood Function", Connection Science, 2010 <1%
Publication

---

36 Zhang, F.. "Effects of thermal oxidative ageing on dynamic viscosity, TG/DTG, DTA and FTIR of SBS- and SBS/sulfur-modified asphalts", Construction and Building Materials, 201101 <1%
Publication

---

37 Kefei Liu, Linfei Deng, Jiayu Zheng. "Nanoscale study on water damage for different warm mix asphalt binders", International Journal of Pavement Research and Technology, 2016 <1%
Publication

---

38 Wu, S.. "Rheological properties for aged bitumen containing ultraviolate light resistant <1%

materials", Construction and Building Materials, 201208
Publication

39	Singh, Maninder, Praveen Kumar, and Mannan Ram Maurya. "Effect of aggregate types on the performance of neat and EVA-modified asphalt mixtures", International Journal of Pavement Engineering, 2014. Publication	<1%

Exclude quotes	On	Exclude matches	< 10 words
Exclude bibliography	On		